Astron. Astrophys. 321, 791–802 (1997)

ASTRONOMY AND ASTROPHYSICS

Spectropolarimetry of symbiotic stars: AG Draconis⋆

H.M. Schmid[1,2] **and H. Schild**[1]

[1] Institut für Astronomie, ETH-Zentrum, CH-8092 Zürich, Switzerland
[2] Mount Stromlo and Siding Spring Observatories, ANU, Weston Creek P.O., ACT 2611, Canberra, Australia

Received 24 July 1996 / Accepted 9 October 1996

Abstract. We present a series of spectropolarimetric observations of the symbiotic system AG Dra and focus on the polarization in the λ6825 and λ7082 lines, which are due to Raman scattering of O VI $\lambda\lambda$1032,1038 emission. The polarization in the Raman lines is variable and the polarization angle shows periodic changes which are linked to the orbital motion even if the object goes into outburst.

From the rotation in the line polarization angle, we find for the orbit inclination $i = 120\,^\circ$ ($105^\circ - 140^\circ$). This implies for a reasonable total mass of the binary system that the hot component's mass lies in the range $0.17 - 0.52\,M_\odot$. This mass is rather low but not in real conflict with the interpretation that the hot component is a CO white dwarf and that the AG Dra system underwent in the past a Barium star type mass transfer episode.

Our observations cover the 1994 outburst phase. During outburst the O VI radiation increased strongly while the Raman scattered radiation remained practically constant. This decrease in Raman efficiency is probably due to a reduction of available H^0 scatterers as a consequence of the enlarged ionization during outburst.

We detect intrinsic continuum polarization which is at least partly locked to the orbital motion and therefore also seems to be induced by a scattering process.

Key words: binaries: symbiotic – circumstellar matter – scattering – polarization – stars: individual: AG Dra

1. Introduction

AG Dra is a bright symbiotic binary at high galactic latitude ($b = 41^\circ$), with high radial velocity ($v_r = -148$ km/s) and a low metallicity of [Fe/H] ≈ -1.3. These properties suggest that it belongs to the halo population.

AG Dra consists of a hot white dwarf ($T_\mathrm{h} \approx 120\,000$ K), and a K-giant. The red giant is enriched in heavy s-process elements like the cool components in binary Barium and CH stars. The hot white dwarf in AG Dra ionizes parts of the cool giant's wind producing a dense emission nebula with strong far UV lines (He II, C IV, N V, O IV], O VI) and H I, He I, He II recombination lines in the visual region. The hot component experienced many 1-3 mag optical eruptions which recur at irregular intervals. The most recent outbursts occurred in 1994, 1985 and 1980.

AG Dra is a well studied symbiotic system. The recent literature includes extensive photometric work (e.g. Kaler 1987; Kaler et al. 1987; Skopal 1994) and many detailed descriptions of the spectroscopic properties and variations (e.g. Viotti et al. 1983, 1984; Iijima et al. 1987; Lutz et al. 1987; Kafatos et al. 1993; Mikolajewska et al. 1995). Several system parameters have been determined, e.g. the orbital period (Meinunger 1979), the binary mass function from radial velocity variations (Mikolajewska et al. 1995; Smith et al. 1996) and the temperature of the hot component (e.g. Mürset et al. 1991; Greiner et al. 1996). Nebular C,N,O abundances have been measured by Schmid & Nussbaumer (1993), and abundances of heavy elements in the cool giant's photosphere by Smith et al. (1996). Mikolajewska et al. (1995) give a comprehensive overview and interpretation of the existing observations for AG Dra.

However, there are also still badly known or controversial values for basic system parameters. These are among others the system distance and therefore its luminosity, the orbital inclination and the stellar masses of the binary components. There exists also a pressing lack of knowledge on the distribution of circumstellar material and the nature of the interaction processes, not only for AG Dra but for the entire class of symbiotic binaries. Clarification of these issues is important for the understanding of the evolutionary status of symbiotic binaries, such as the possibility of being progenitors of type Ia supernovae (e.g. Kenyon et al. 1993) or the connections between symbiotic binaries and Barium star type binaries (Schmid 1994; Smith et al. 1996).

In this paper we present for AG Dra a series of spectropolarimetric observations of the Raman scattered emission lines $\lambda\lambda$6825,7082 in order to determine the orbital inclination, to

Send offprint requests to: H. Schild

⋆ Based on observations obtained with the William Herschel Telescope of the Royal Greenwich Observatory, La Palma, Canary Islands

estimate stellar masses and to give new constraints on the geometry of the circumstellar material.

The strong, broad emission lines at λ6825 and λ7082 are produced by a Raman scattering process of the O VI $\lambda\lambda$1032,1038 resonance lines by neutral hydrogen (Schmid 1989). In symbiotic systems it is expected that strong O VI emission lines are produced in the ionized region near the hot component. They are converted into $\lambda\lambda$6825,7082 by neutral hydrogen in the extended atmosphere of the cool giant. Raman scattering is a dipole type scattering process which produces strong light polarization in the O VI Raman lines (Schmid & Schild 1990, 1994; Harries & Howarth 1996b). The polarization signal in the Raman lines is expected to be locked to the binary motion, and can be used for determining the orbital inclination and the orientation of the line of nodes (Schmid 1992; Schild & Schmid 1996; Harries & Howarth 1996a). In addition, the line polarization structure in $\lambda\lambda$6825,7082 contains important information on the location of the O VI region and on the geometric and dynamic structure of the H^0-scattering region (Schmid 1996; Harries & Howarth 1996c).

Here we present results from a spectropolarimetric monitoring program of a few northern symbiotic systems (Schild & Schmid 1992, 1996). Section 2 describes the observations and Sects. 3 and 4 present the data. This is followed by an analysis of the observed variations in Sect. 5 and the determination of a polarimetric orbit in Sect. 6. We discuss our findings in Sect. 7.

2. Observations

We monitored the AG Dra system spectropolarimetrically with the 4.2m William Herschel Telescope and the ISIS spectrograph. The data were collected by RGO support astronomers as service observations. The first of these observations was described in Schmid & Schild (1994, hereafter Paper I) where the observational details can be found. They were taken with the 600R grating and suffered from a considerably degraded spectral resolution because of a focusing error. The other observations were obtained with the 1200R grating which provided a resolution of 0.65 Å. The detector was a coated EEV CCD with 1242×1152 pixels each 22.5 μm square except for the last two observations where a TEK CCD with 1024×1024 with 24 μm pixels was used. The wavelength coverage was from 6730 Å to 7190 Å. The slit was 1″ wide and kept in a fixed direction on the sky. A dekker with three apertures, one for the object and two for the sky, was used.

A rotatable half-wave plate can be inserted into the beam and each measurement of linear polarization consists of a set of four observations taken at angles of 0°, 22.5°, 45° and 67.5°. A calcite block located below the slit generates two beams with perpendicular polarization. Normally two cycles with exposure times of 10 min in each half-wave setting were obtained. Exposures with the half-wave plate at 0° and 45° yield Stokes Q whereas the other two yield Stokes U. The details about how the polarization signal was extracted can be found in Paper I.

A number of polarization standard stars were observed during each night such that instrumental polarization effects could be removed. The instrumental polarization was usually found to be of the order of 0.1 %.

The observed linear polarization, described by the parameter set (I, Q, U, p, γ), consists of the intrinsic polarization for the line and continuum radiation and the interstellar polarization induced by dust grains. As in Paper I we use the indices ℓ and c for the measured line and continuum polarization, respectively. The intrinsic polarization, after correction for the interstellar polarization, is correspondingly denoted with the indices L and C.

3. Equivalent widths and line structure

Our eight spectropolarimetric observations of AG Dra were taken between Aug 1991 and July 1995 in irregular intervals (Tables 1 and 2). During this time AG Dra had an outburst starting in June 1994, followed by a slow and steady decline and a secondary outburst near our last observations in July 1995. Table 1 includes V magnitudes for our observations to illustrate the connection with the light curve history.

For the orbital phase we adopt the photometric ephemeris of Meinunger (1979) for the maxima in the U filter

$$\mathrm{JD(U_{max})} = 2\,438\,900 + 554 \times \phi\,.$$

Further photometric studies confirm that this ephemeris is very accurate with an uncertainty of less than about ±3 days in the period P and about ±12 days in the maximum epoch T_0 (Kaler 1987; Skopal 1994). Periodic radial velocity variations have been measured for the cool giant in AG Dra by Garcia & Kenyon (1988), Mikolajewska et al. (1995) and Smith et al. (1996). These papers demonstrate that conjunctions occur close to photometric minima and maxima.

3.1. Raman equivalent widths and fluxes

Table 1 gives our measured emission line equivalent widths (EWs) for the Raman lines and He I λ7065. They were corrected for the underlying stellar absorption features. These corrections are larger for λ7082, less important for λ6825, and negligible for the narrow He I line. They amount to +0.3Å for EW(λ6825) and +0.6Å for EW(λ7082) for all observations. The accuracy of the EW-values is about 5% for λ6825 and He I and 10% for λ7082.

The mean ratio between the equivalent widths of the two components is EW(λ6825)/EW(λ7082) = 2.4±0.3. This value can also be adopted for the line flux ratio $F(\lambda6825)/F(\lambda7082)$ because the stellar continuum is practically constant between 6800Å and 7100Å.

Table 1 lists interpolated and rounded V magnitudes for our observing dates from available photometric measurements. They can be used to convert the EWs into line fluxes. The continuum flux F_c at 6900 Å is according to the photometric studies of Kaler (1987) and Kaler et al. (1987) $F_c = F_V + 2.5(\pm0.5) \cdot 10^{-13}\,\mathrm{erg\,cm^{-2}s^{-1}Å^{-1}}$ during both the quiescent state and the entire 1980-outburst. The available photometry suggests that

Table 1. Emission line equivalent widths in Å for the Raman scattered lines and He I λ7065. The visual magnitudes m_V are derived from the literature and the line flux $F(6825)$ from EW(6825) and m_V as described in the text.

Obs.	JD	m_V	EW [Å]			F^*_{6825}
	244...		λ6825	λ7082	He I	
004	8487.4	9.8[a]	6.4	3.1	1.1	4.2
401	9135.5	9.8[b]	7.7	3.3	1.8	5.0
501	9190.4	9.8[b,c]	11.6	4.9	3.6	7.5
601	9202.5	9.8[b,c]	13.6	5.4	4.0	8.8
701	9222.4	9.8[b,c]	16.2	6.0	4.8	10.5
	9499.5	9.8[d]				
	9506.5	9.3[d]	start of outburst			
	9518.1	8.4[d]	1994 outburst maximum			
1001	9614.4	9.0[c]	5.2	2.7	2.8	5.7
1201	9795.7	9.5[e]	5.5	2.3	2.8	4.3
1301	9914.6	9.1[e]	9.5	3.8	4.0	9.6

$*$: in 10^{-12} erg cm^{-2}s^{-1}

a: Skopal et al. (1992); b: Hric et al. (1994); c: Skopal et al. (1995); d: Granslo et al. (1994) visual magnitudes; e: Skopal (1996)

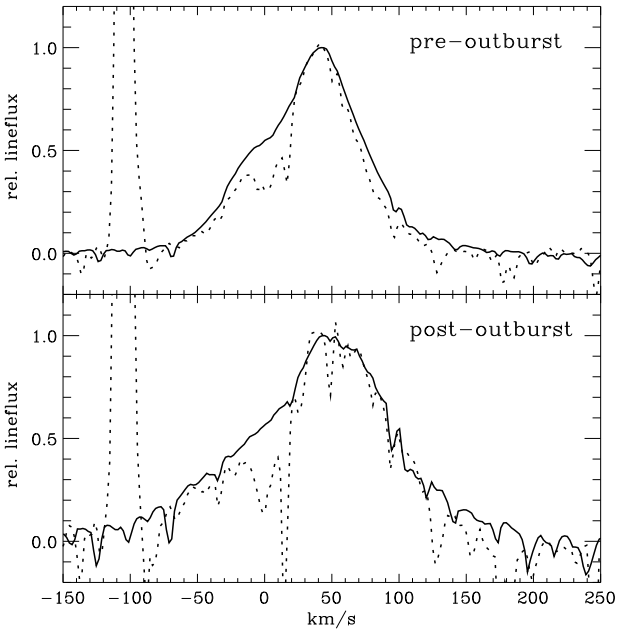

Fig. 1. Line structure of the Raman lines λ6825 (solid line) and the λ7082 (dotted line) in the velocity space of the original O VI lines (corrected for the system motion of AG Dra). The upper panel shows data from 1993 Aug. 22 and the lower panel from 1994 Sep. 18, about 100 days after the June 1994 outburst The profiles are not corrected for photospheric and telluric absorptions.

this relationship holds also for our observing epoch. Thus a quiescence luminosity of m_V = 9.8 transforms into a continuum flux of about $F_c = 0.65(\pm0.10) \cdot 10^{-12}$ erg cm^{-2}s^{-1}Å^{-1} and accordingly higher for outburst observations. Table 1 gives line fluxes for the λ6825 Raman line derived with this procedure. Fluxes for λ7082 and He I can be obtained by using the same scaling factor. We estimate that the error in the EW–line flux conversion is about 20%.

The λ6825 flux varied by about a factor of 2.5 during our observing period. Previous data series confirm that the λ6825 line strength remains in this range over much longer time scales (Iijima et al. 1987; Mikolajewska et al. 1995). Thus the O VI Raman lines show much weaker flux variations than the strong far UV emission lines such as He II, C IV and N V (e.g. Viotti et al. 1984).

3.2. Raman line structure

The O VI Raman lines in AG Dra have a profile with a red peak and a blue shoulder (Fig. 1). Similar profiles are seen in the symbiotic systems HK Sco, CD−43°14304 and Hen 1342. They contain, like AG Dra, a K giant or an early type M giant. Symbiotic systems with late M giants or Mira variables show more structured Raman line profiles with two or even three intensity peaks (see Allen 1980; Harries & Howarth 1996b).

The Raman line shapes in AG Dra varied usually only slightly (Fig. 2). An exception are the first data taken after the outburst, which show wider lines with a substantially different structure (Fig. 1). No obvious differences are visible between the line profiles of the λ6825 and the λ7082 components. The differences in Fig. 1 are mainly due to strong photospheric lines from the K-giant and some telluric absorptions superimposed on the Raman lines, especially the λ7082 component.

The full line width at 25% of the peak line intensity (FW25%) is $\Delta\lambda_{\rm Ram}$ = 18(±2) Å for all observations except for Sep 1994 where the line widths are $\Delta\lambda_{\rm Ram}$ = 28 Å. From these Raman line widths we can estimate the widths of the original O VI $\lambda\lambda$1032,1038 lines according to

$$\Delta\lambda_{\rm OVI} = \left(\frac{\lambda_{\rm OVI}}{\lambda_{\rm Ram}}\right)^2 \Delta\lambda_{\rm Ram}\,, \qquad (\text{for } \Delta\lambda \ll \lambda)$$

where $\lambda_{\rm OVI}$ and $\lambda_{\rm Ram}$ are the vacuum wavelengths of the original O VI lines 1031.93 Å and 1037.62 Å and the corresponding Raman transition 6827.32 Å and 7084.35 Å (Schmid 1989). Thus, a Raman line width of $\Delta\lambda_{\rm Ram}$ = 18 Å translates into a line width of $\Delta\lambda_{\rm OVI}$ = 0.41 Å, or a velocity width of Δv = 120 km s^{-1}, for the original O VI lines. The corresponding values for the post-outburst observations of Sep. 1994 are $\Delta\lambda_{\rm OVI}$ = 0.64 Å and Δv = 185 km s^{-1}.

The Raman lines in AG Dra exhibit also a systematic red shift of about 6 Å (±1 Å). This corresponds to a red shift of 0.14 Å for the original O VI lines or a velocity shift of 40 km s^{-1} with respect to the systematic velocity of the system (−148 km s^{-1}).

The derived line widths $\Delta\lambda_{\rm OVI}$ and mean velocity shift neglect the Doppler shifts which are introduced by the systematic motion of the Raman-scattering H^0-atoms in the red giant wind. This effect produces an extra contribution to the Raman line widths and probably a small systematic red shift of the mean wavelength of the Raman lines (see Schmid 1996). Typical wind

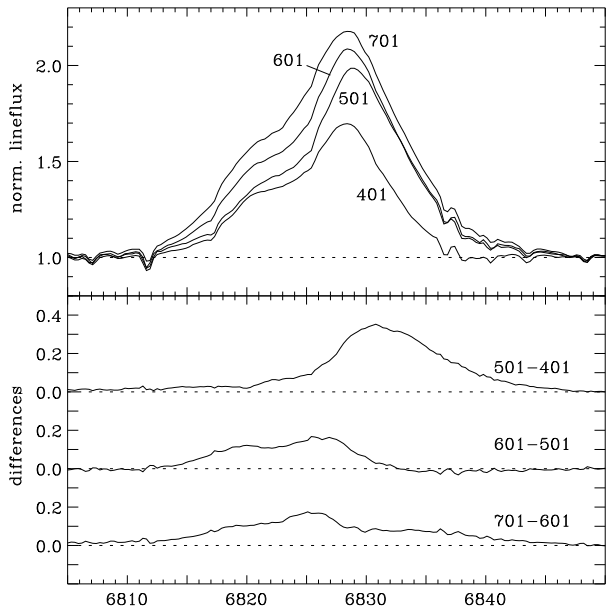

Fig. 2. Temporal changes of the line structure λ6825 for the observations 401, 501, 601 and 701 taken within 3 months in 1993. The lower panel shows the flux differences between subsequent observations.

velocities for cool giants are about 10 km s^{-1}. Thus, the real line width and the systematic red shift of the far UV O VI lines may be reduced by such an amount.

Are these line widths and velocity shifts reasonable for the O VI emission lines of AG Dra? We have only circumstantial evidence on the O VI line structure, as no high resolution observations exist. But our determinations of the O VI line structure are in very good agreement with high resolution IUE observations of the N V $\lambda\lambda$1239,1243 resonance lines (Viotti et al. 1983, 1984). They measure a line width (full width at half maximum) of about 0.30 Å (Δv = 73 km s^{-1}), which represents a firm lower limit for the full widths at 25% of the peak line intensity. The systematic red shift of N V, with respect to the intercombination lines, lies in the range $10 - 30$ km s^{-1} or $0.04 - 0.12$ Å.

A systematic red shift in N V and other UV resonance lines, like C IV and Si IV, is commonly observed in symbiotic systems (Friedjung et al. 1983). This property is explained by a P Cygni-like radiative transfer effect in an expanding medium.

Figure 2 shows the variations in the λ6825 line structure for the 1993 observations, which were taken within 3 months (16% of the orbital period) and precede the 1994 outburst. They show a steady increase in the Raman intensity, first in the red wing and followed by central and blue enhancements. The first observation of this subsample was taken near photometric minimum. The evolution for the later observations could therefore be interpreted as egress phase of a partial obscuration of the Raman scattering region. In this case we would see first the egress of a scattering region which predominantly produces Raman photons in the red line wing (difference 501–401). This phase is followed by the egress of a region from which central and blue Raman photons originate. Alternatively, the line flux enhancement could be related to fluctuations in the O VI irradiation. Support for this interpretation comes from photometric measurements which indicate for the 1993 season stronger emission in the U and B band ($\approx$ 1 mag) coupled with relatively strong irregular variations (see Greiner et al. 1996).

Table 2. Mean continuum polarization in the interval λ6860 – λ7040. The position angle γ_c is given in degrees (North over East), the polarization p_c and the normalized Stokes parameters as a percentage. ϕ is the photometric phase of the observation.

Obs.	Date	ϕ	p_c	γ_c	Q_c/I_c	U_c/I_c
004	17-8-1991	17.306	0.24	92	–0.24	–0.02
401	27-5-1993	18.476	0.21	89	–0.21	0.01
501	21-7-1993	18.575	0.27	59	–0.13	0.24
601	02-8-1993	18.597	0.16	38	0.04	0.16
701	22-8-1993	18.632	0.02	13	0.02	0.01
1001	18-9-1994	19.340	0.32	107	–0.26	–0.18
1201	18-3-1995	19.667	0.05	101	–0.05	–0.02
1301	16-7-1995	19.882	0.16	88	–0.16	0.01

4. Raman polarization

4.1. Observed continuum polarization

The Raman lines produce a strong polarization signal. Outside the Raman lines the polarization is small and wavelength independent in the spectral range covered. Table 2 lists our measured continuum polarizations which are also plotted in the $Q/I - U/I$-plane in Fig. 3. The given values are flux weighted means for the interval 6860–7040 Å. Previous polarimetric data of AG Dra were taken by Schulte-Ladbeck (1985) in 1983. She obtained a polarization of 0.24 ± 0.04 % and 91° in the V-band filter and similar values in other filters.

The continuum polarization shows temporal (intrinsic) variations which are larger than the estimated measuring errors of about $\pm 0.1\%$ in Q_c/I_c and U_c/I_c. Especially the measurements from 1993 (401, 501, 601, 701) exhibit a retrograde rotation in the $Q/I - U/I$-plane which is similar to the rotation seen in the Raman lines (Fig. 3). Also the observation for Sep 1994, our first data after the 1994 outburst, show a significantly different polarization compared to previous measurements. An enhanced continuum polarization of 0.4% after the 1994 outburst is also reported in Garnavich & Trammell (1995).

The presence of an intrinsic continuum polarization makes an assessment of the interstellar polarization difficult. Only few determinations of the interstellar polarization in the vicinity of AG Dra exist (see Schmid & Schild 1994). They suggest a polarization of about $p_{\rm is} = 0.1\%$ and $\gamma_{\rm is} = 90°$ in this sky region. This estimate is based on measurements of stars which are, on average, much closer to us than AG Dra. Thus, the real interstellar polarization for AG Dra is most likely larger. We estimate for the interstellar polarization $q_{\rm is} = -0.2 \pm 0.1\%$, $u_{\rm is} = 0.0 \pm 0.1\%$ ($p_{\rm is} = 0.2\%$, $\gamma_{\rm is} = 90°$). This value implies that the intrinsic polarization is very small ($p_C \lesssim 0.1\%$) for our observations

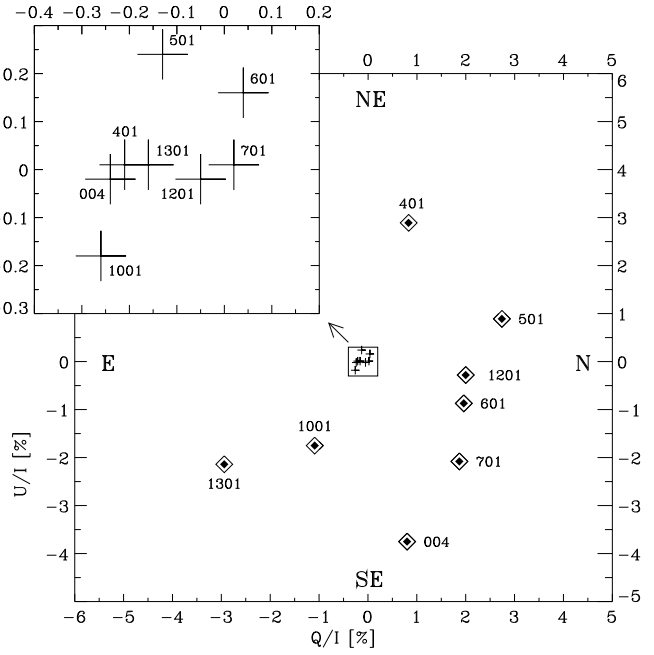

Fig. 3. Stokes parameters for the continuum polarization $Q_c/I_c, U_c/I_c$ (crosses) and the λ6825 line polarization Q_ℓ/I_ℓ, U_ℓ/I_ℓ (diamonds). Each point is identified by the corresponding observation number. The estimated measuring errors are of the size of the crosses (continuum) and of the inner filled diamonds (line).

004, 401 and 1301 as well as for the measurement of Schulte-Ladbeck (1985).

The weakness of the continuum polarization and the large uncertainties in the interstellar polarization make an interpretation of the intrinsic continuum polarization in AG Dra difficult. However our data proof that a variable intrinsic continuum polarization is present in AG Dra, which has not been recognized previously (Schulte-Ladbeck et al. 1990). Further, the temporal changes in the continuum polarization shows a pattern in the $Q/I - U/I$-plane which is similar to the polarization in the Raman lines (Fig. 3). For example, in 1993 the continuum polarizations (data points 501, 601 and 701) show a retrograde (clockwise) rotation like the line polarization. Also the Q_c/I_c, U_c/I_c-measurements 1001 and 1201 suggest a relation between the position angle γ_C for the intrinsic continuum polarization and the γ_ℓ for the line polarization.

4.2. Observed Raman line polarization

In order to properly determine the polarization in the Raman scattered lines, careful separation of the photospheric emission (I_c) and line emission ($I_\ell = I - I_c$) is necessary. The stellar absorptions in the λ6825 line are weak and their correction with a spectrum of a comparison star of similar spectral type was straightforward. More difficult was the subtraction in the λ7082 component, where the stellar absorptions are stronger and additionally contaminated by telluric lines.

After photospheric subtraction the normalized Stokes parameters for the Raman lines were extracted in the same way as in Paper I with

$$\frac{Q_\ell}{I_\ell} = \frac{I}{I_\ell}\Big(\frac{Q}{I} - \frac{Q_c}{I_c}\frac{I_c}{I}\Big)$$

and similarly for U_ℓ/I_ℓ. Note that the ratio Q/I is the measured polarization spectrum and Q_c/I_c the continuum polarization determined in Sect. 3.4 (Table 2). Of course the relative line parameters Q_ℓ, U_ℓ and p_ℓ are only defined where the line flux I_ℓ is not zero.

In addition, we should correct the measured line polarization (Q_ℓ, U_ℓ) for the interstellar polarization in order to obtain the intrinsic line polarization (Q_L, U_L). As described in the previous section, the interstellar polarization for AG Dra is not well determined, but certainly very small ($\approx 0.2\%$) when compared to the typical line polarization of about 3% (see also Fig. 3). The interstellar correction would be smaller than the measuring accuracy for the line polarization and its effect on the results obtained below is negligible. Therefore, we do not apply any correction for the interstellar polarization.

Figure 4 shows the spectropolarimetric line structure for the λ6825 component for all our observations. The panels give the intensity I, the "rotated" Stokes parameters Q'_ℓ and U'_ℓ, the percentage polarization p_ℓ and the polarization angle γ_ℓ. Q'_ℓ and U'_ℓ are the Stokes parameters in a coordinate system which has been aligned with the mean polarization angle $\langle\gamma\rangle$ in the λ6825 Raman line. This means, that the U'_ℓ-parameter integrated over the entire λ6825 feature is zero. The mean position angle $\langle\gamma\rangle$ is indicated in the panels.

The percentage polarization p_ℓ and the polarization angle γ_ℓ in four wavelength bins of 5 Å width are listed in Table 3 together with polarization values for the integrated Raman lines.

A comparison between the Raman lines λ6825 and λ7082 shows that the polarization signal behaves very similar in both components. The only obvious systematic difference is, that the λ6825 component shows in all except the first observation (where the reduced resolution precludes an accurate subtraction of the photospheric absorptions) a smaller polarization than the λ7082 component. The mean difference in the total polarization excluding observation 004, is $\langle\Delta p\rangle = -1.2\%$ ($\sigma_{\Delta p} = \pm 0.3\%$). The integrated polarization angles reveal no significant difference $\langle\Delta\gamma\rangle = -1^\circ$ ($\sigma_{\Delta\gamma} = \pm 6^\circ$) between the λ6825 and λ7082 components. The above standard deviations $\sigma_{\Delta p}$ and $\sigma_{\Delta\gamma}$ for the polarization differences between the two components λ6825 and λ7082 can be considered as upper limits to the measuring uncertainties in our data.

5. Correlations

In principle, AG Dra offers the opportunity to examine the Raman polarization properties in relation to orbital motion as well as to parameters associated with the outburst which occurred in 1994. Due to the limited data set, it is however often not entirely clear how to separate orbital from outburst effects. Below

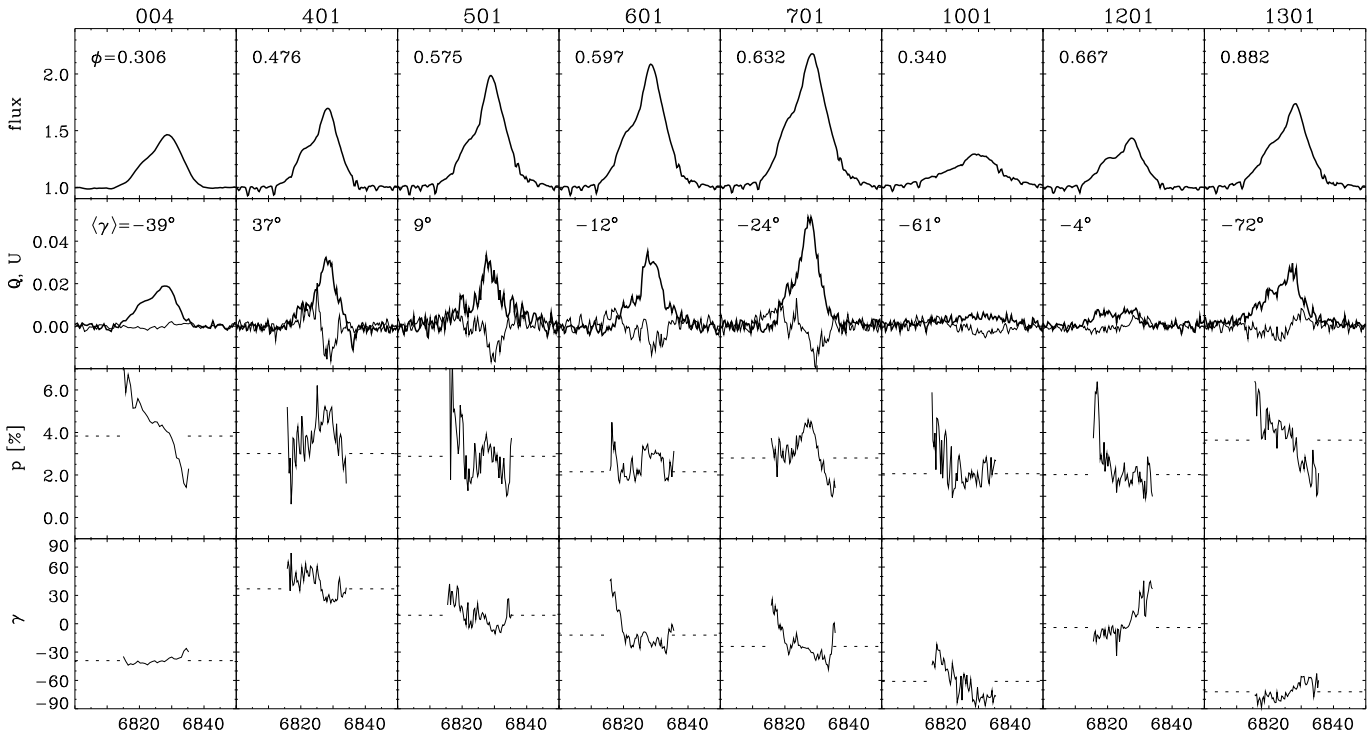

Fig. 4. Normalized flux I, rotated Stokes parameters Q'_ℓ (bold) and U'_ℓ, percentage polarization p_ℓ and position angle γ_ℓ for the λ6825 line in AG Dra for all our WHT observations. The alignment of the $Q' - U'$ system (for each individual measurement) is equal to the flux weighted mean of the polarization angle $\langle\gamma\rangle$ as indicated in γ_ℓ by a dashed line. Thus, the integrated U'-parameter vanishes in that system. The dashed line in the p-panel gives the flux weighted (mean) percentage polarization.

Table 3. Flux weighted polarization in the λ6825 (upper Table) and the λ7082 (lower Table) lines. Values are given for the entire line and 4 subintervals corresponding to the extreme blue, blue, red, and extreme red portions of the Raman lines.

Obs.	total		[6815–6820]		[6820–6825]		[6825–6830]		[6830–6835]	
	p_ℓ	γ_ℓ	p_ℓ	γ_ℓ	p_ℓ	γ_ℓ	p_ℓ	γ_ℓ	p_ℓ	γ_ℓ
004	3.83	141	5.6	139	4.7	139	4.2	141	2.7	145
401	3.01	37	2.9	47	3.7	54	4.5	32	3.0	31
501	2.88	9	4.9	26	2.3	8	3.1	2	2.1	177
601	2.15	168	2.1	19	2.0	162	2.9	164	2.5	161
701	2.80	156	2.8	3	3.2	158	4.1	151	2.1	145
1001	2.06	119	3.5	143	1.9	118	1.7	109	2.2	101
1201	2.02	176	3.6	167	2.0	172	1.9	5	1.4	31
1301	3.64	108	4.8	102	4.2	101	3.4	110	2.2	119

Obs.	total		[7072–7077]		[7077–7082]		[7082–7087]		[7087–7092]	
	p_ℓ	γ_ℓ	p_ℓ	γ_ℓ	p_ℓ	γ_ℓ	p_ℓ	γ_ℓ	p_ℓ	γ_ℓ
004	2.61	139	4.4	121	4.1	140	5.3	142	3.0	143
401	4.35	51	1.4	64	4.5	48	5.9	51	3.4	49
501	3.34	8	7.0	16	1.9	175	3.2	1	2.5	5
601	3.23	168	2.6	10	2.4	165	3.8	163	3.2	160
701	4.10	159	4.9	179	3.3	157	5.5	151	3.0	149
1001	3.56	112	2.6	117	2.4	110	3.4	105	3.3	104
1201	3.42	178	4.3	165	2.8	172	2.9	6	3.6	22
1301	4.87	109	8.3	102	4.5	94	4.8	115	4.1	123

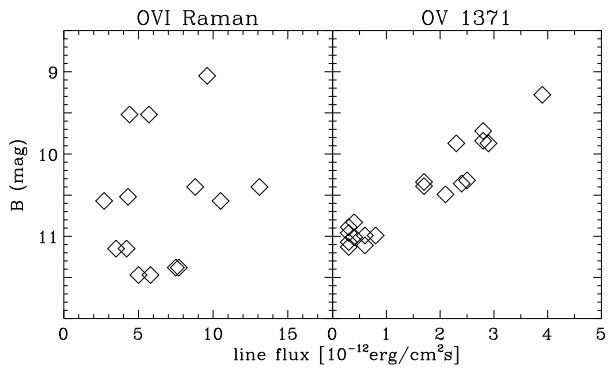

Fig. 5. Correlation between the O VI λ6825 Raman line (left) respectively the O V λ1371 recombination line (right) and B-magnitudes. Line fluxes are taken from Table 1 and from Mikolajewska et al. (1995).

we summarize some facts and interpretations which still can be made.

5.1. Raman intensity

The flux in the Raman features shows no regular trend, neither in our data nor in previous flux measurements of Mikolajewska et al. (1995) and photographic data of Iijima et al. (1987). The existing observations suggest that the line strength of λ6825 remains around $7 \cdot 10^{-12}$ erg cm^{-2}s^{-1} with a scatter of about $\sigma = \pm 3 \cdot 10^{-12}$ erg cm^{-2}s^{-1}.

Orbital effects seem to be unimportant for the light curve of the Raman lines. We have mentioned the possibility of an eclipse phase in our 1993 measurements (Sect. 3.2) which is, however, questionable. With respect to outbursts we note that the Raman flux prior to the outburst was about a factor of 2 higher than 108 and 280 days after maximum. Such a decrease is however not considerably larger than the fluctuations which are also observed during quiescent phases.

Thus, the Raman line fluxes $\lambda\lambda$6825,7082 also do not seem to be correlated with the outburst light curve. This is an outstanding property because "normal" UV and optical emission lines show a strong correlation with luminosity. Typically, the emission line fluxes, e.g. He II λ1640, O III] λ1664, C IV λ1550, N V λ1240 or O V λ1371, increase during outbursts by factors of 3 to 10 over the mean quiescent level (see e.g. Kafatos et al. 1993; Mikolajewska et al. 1995; Greiner et al. 1996).

Figure 5 shows the correlations between B magnitudes and the λ6825 Raman line fluxes as well as the O V λ1371 line fluxes. There clearly is no correlation between λ6825 and B, but a very strong one between O V and B. Because O V λ1371 is a recombination line from the O^{+5} ion, it mirrors the O VI $\lambda\lambda$1032,1038 intensity. The λ6825 fluxes were measured between 1984 and 1995 (Mikolajewska et al. 1995 and Table 1) and the O V fluxes between 1979 and 1987 (see Mikolajewska et al. 1995). During the 1994 outburst the UV emission lines, including O V, showed a very similar behaviour as for the 1980 outburst (Greiner et al. 1996). B-magnitudes are a good tracer of the activity in AG Dra and measurements contemporary ($\pm$10 days typically) to the emission line fluxes where taken from the literature cited in Table 1 and from Hric et al. (1993).

We conclude from Fig. 5, that the O VI intensity increases strongly during outbursts (say, by a factor between 3 and 10) while the Raman scattered radiation is hardly changed. In outburst, the Raman scattering efficiency is thus considerably reduced. This decrease must be connected to a strong reduction in the number of neutral scatterers. We note that the optical brightening indeed is dominated by a sudden increase of nebular continuum emission, indicating that large amounts of material become newly ionized and thus are no longer able to scatter O VI radiation.

Due to these changes in the scattering situation we might also expect drastic changes in the polarization signal. In order to assess possible relationships we have correlated the measured polarization with the equivalent width and absolute flux of λ6825, the visual magnitude and orbital phase.

5.2. Polarization angle

All polarization angles listed in Table 3 correlate well with orbital parameters like radial velocity or phase. Corresponding linear correlation coefficients lie around 0.9 or higher. The rotation as a function of time is clock-wise for all angles. Additionally, observations from different cycles fit the same relation. It is clear that the factor dominating all polarization angles is orbital motion. There remain however deviating residuals from a strict relation which are larger than the observational errors. There must thus exist a second order effect which produces deviations of the order of $\pm 20\,^\circ$.

Interestingly, also the angle of the continuum polarization shows a clear correlation with orbital motion and can therefore not be due to interstellar polarization. Possible formation mechanisms must involve a scattering effect which is linked to the binary orientation (see Sect. 4.1).

5.3. Percentage polarization

The percentage polarization is not linked in an obvious way to orbital motion. For an inclined orbit we expect the polarization to follow a curve resembling a double sine wave over one orbital period with minima at conjunction and maxima at quadrature phases (see Schmid 1992, 1996; Harries & Howarth 1996c). The amplitude of these variations depends on the inclination. For example, the model calculations mentioned above suggest variations in p_ℓ between zero and a maximum value $p_{\rm max}$ for an inclination of $i = 90^\circ$, between about $p_{\rm max}/2$ and $p_{\rm max}$ for $i = 45^\circ$ (or 135°), and no variations in the percentage polarization in the case of a pole-on orbit ($i = 0^\circ$ or 180°).

Contrary to this, the measured polarization varies in an erratic way between 2.0% and 3.8% in the λ6825-component and between 2.6% and 4.9% in the λ7082 component. A possible interpretation could be a superposition of a "regular" double wave curve for a sin$i$ smaller than about 0.7 and irregular fluctuations with an amplitude of at least 1% in p.

5.4. Line polarization structure

The line profiles show a rotation in the polarization angle of up to 45° from the blue to the red wing. We observe two qualitatively different Raman polarization profiles:

- The polarization angle rotates counter-clockwise and the percent polarization steadily decreases as one moves across the profile from blue to red. Such profiles were observed at the beginning (004) and the end of our series (1201, 1301).
- The angle profiles are either flat or rotate clockwise. The percent polarization is characterized by a polarization maximum in the central/red part of the Raman line (Fig. 4). Such profiles were seen previous to the outburst (401, 501, 601 and 701).

The first polarization profile obtained after the outburst (1001) combines features from both profile types: The angle rotates clockwise but the percentage polarization has a turning point and rises again in the red part.

Whether these differences are determined by orbitally or outburst-related factors remains an open question. The division of the two classes into pre- and post-outburst periods indicate that at least a partial influence must come from the outburst activity. The wavelength dependent rotation, on the other hand, is clock-wise for orbital phases between 0.34 and 0.64 and anticlock-wise for the other observations. This may suggest that obscuration effects near the conjunction phase 0.50 (hot component behind cool giant) could also play a role.

We note that the two observations just after the outburst had small percentage polarizations in the line center. Since these parts dominate the flux, the polarization in the integrated line is also reduced. The percentage polarization in the line wings does not seem to be smaller after the outburst.

6. Polarimetric orbit for AG Dra

Phase locked polarization from a binary system can, in principle, be used to determine 3-d orbits. The technique has been developed by Rudy & Kemp (1978) and Brown et al. (1978) and was mainly applied to massive binary systems (e.g. Robert et al. 1990 and references therein). For example, the polarization in these systems is produced by Thomson scattering in the extended atmosphere of the Wolf-Rayet component which is irradiated by the hot companion O star.

With the discovery of Raman scattering occurring in symbiotic systems (Schmid 1989), the same technique becomes applicable to low mass binaries. First results have already been published for SY Mus (Harries & Howarth 1996a) and V1016 Cyg (Schild & Schmid 1996). In the case of AG Dra, radial velocity and photometric measurements are consistent with a circular orbit with a period close to 554 days. In the following we discuss how the orbit inclination and orientation on the sky can be deduced from our polarimetric observations.

Table 4. Least square solutions for the angle of the line of nodes Ω and the inclination i for circular orbits with fixed period P = 554 days and 3 different conjunction epochs T_0.

used line section	Ω	i	σ	
T_0 = 2 448 276 (polarimetric phase)				
λ6825 total	163	116	8.2	$*$
6815–6820 xblue	175	125	8.0	
6820–6825 blue	163	122	9.7	
6825–6830 red	160	115	12.4	
6830–6835 xred	162	113	22.1	
λ7082 total	164	122	9.7	
7072–7077 xblue	168	145	4.7	
7077–7082 blue	159	122	9.0	
7082–7087 red	163	119	14.8	
7087–7092 xred	166	118	19.7	
T_0 = 2 448 305 (radial velocity phase)				
λ6825 total	146	121	11.4	
λ7082 total	147	123	9.6	
T_0 = 2 448 318 (photometric phase)				
λ6825 total	137	126	13.6	
λ7082 total	139	125	11.0	

$*$: solution plotted in Figs. 6 and 7

6.1. Orbit inclination and orientation

We have calculated "polarimetric orbits" i.e. fitted a projected circular orbit to the observed polarization angles. Free parameters are the period P, the time of the conjunction phase T_0, the line of nodes of the orbital plane Ω and the orbital inclination i. The best solution (least squares) with the only constraint that $100 < P$ [days] < 1000 yields $P = 555^d$, $T_0 = 8276$, $\Omega = 162°$, $i = 117°$, $\sigma = 8.2°$ for the integrated λ6825 line and $P = 554^d$, $T_0 = 8290$, $\Omega = 156°$, $i = 122°$, $\sigma = 8.9°$ for the integrated λ7082 line. σ is the standard deviation of the measured polarization angles from the fit solution. An inclination $90° < i \leq 180°$ stands for a retrograde (or clockwise) binary rotation. It is noteworthy that the polarimetric periods for both lines lie extremely close to the photometric period. The high accuracy of the polarimetric period from only 8 measurements comes from the fact that an uncertainty of about 10° in the orientation of the binary axis (e.g. due to fluctuations in the alignment of the scattering geometry) is small compared to a 360° rotation during one period or the 900° rotation covered by our measurements.

Also the resulting T_0 turn out to be in good agreement with the conjunction phase $JD_{244} = 8318 \pm 12$ from photometric light curves (Meinunger 1979; Skopal 1994), or $JD_{244} = 8305 \pm 16$ from radial velocity curves (Mikolajewska et al. 1995).

For the following discussion we adopt a period P = 554 days. Orbital solutions for various epochs T_0 are summarized in Table 4. Figure 6 shows the measured polarization angle as function of polarimetric phase (bottom axis) and photometric phase (top axis). The thick solid line is the best fitting polarimetric orbit. The dotted line is the corresponding pole-on orbit ($i = 180°$) through the quadrature and conjunction angles of

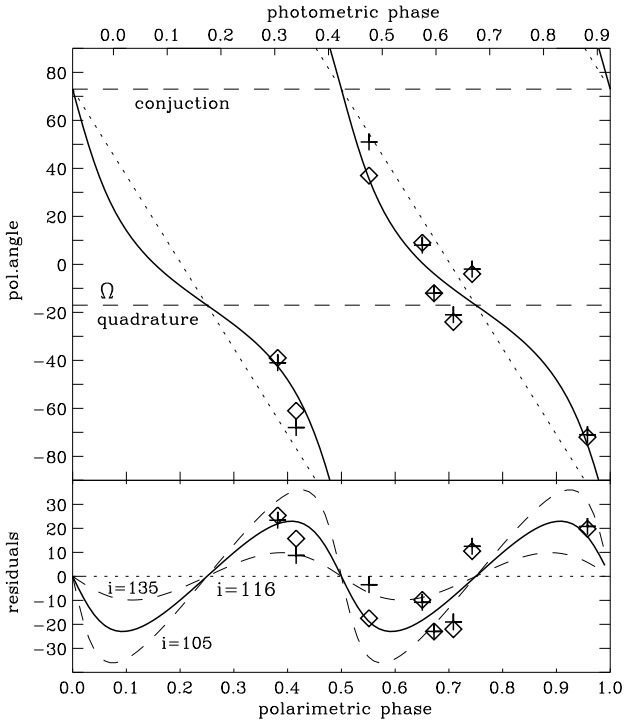

Fig. 6. Measured polarization angle as function of orbital phase for the Raman lines λ6825 (diamonds) and λ7082 (crosses). The solid line is the best fit solution Ω = 163°, i = 116° for the integrated λ6825 polarization angles. The dotted lines give the comparison curve for a pole-on orbit i = 180°. The lower panel shows the residuals with respect to the pole-on orbit. Also shown are the residuals for fits with i = 105° and 135° (dashed lines).

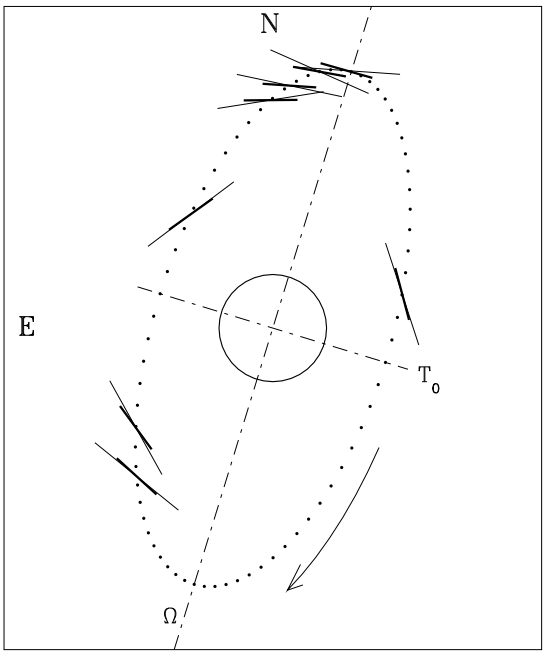

Fig. 7. Polarimetric orbit (Ω = 163°, i = 116°) of AG Dra for the (total) λ6825 feature. The position of the hot component relative to the cool giant is given by dots at ω = 5° intervals. Short thick lines show the calculated position angles at the times of observations, and long thin lines the measured position angles.

the inclined orbit. The lower panel in Fig. 6 gives the residuals of the measured angles and the best fit relative to the pole-on orbit. It is clearly visible, that the residuals of the measured points are positive for phase intervals $0.25-0.5, 0.75-1.0$ and negative for $0.5-0.75$ as expected for an inclined orbit. The geometric meaning of this is that the projected binary axis rotates faster around conjunction phases and slower around quadrature phases.

Figure 7 gives a geometric representation of the spectropolarimetric orbit as projected onto the sky. For this it was assumed that the mean polarization angle $\langle\gamma\rangle$ in the Raman lines is perpendicular to the binary axis (the line connecting the two stars). This is expected for a geometry where the neutral scattering region is located near the cool giant and where the O VI radiation originates from near the hot component (see e.g. Schmid & Schild 1994). Note, that spectropolarimetric data are invariant to a 180°-rotation of the scattering geometry. Thus the orbit plotted in Fig. 7 could also be rotated by 180° on the celestial sphere which leaves an ambiguity in the position of the ascending and descending nodes but does not change the orientation of the line of nodes.

6.1.1. Uncertainties

We assume for an estimate on the orbital inclination i and the orientation of the line of nodes Ω that the scattering geometry mirrors, on average, the orientation of the binary axis. Further we assume that the scatter in the measured polarization angle is due to a random deviation of the scattering geometry from a mean configuration.

The uncertainty in the inclination i can be estimated from a comparison of fit solutions with different i. The residual plot in Fig. 6 suggest that i = 105° and i = 135° are reasonable uncertainty limits for the inclination. The corresponding standard deviation (σ = 13°) is significantly enhanced when compared to the best fit solution for i = 116° (σ = 8.2°).

Further, we should consider the effect of the uncertainty in the conjunction epoch T_0. Different values are determined from photometric, radial velocity and polarimetric data. These may reflect insufficient accuracy in the measurements but could also point to systematic shifts between the orientation of the binary axis and the scattering geometry or to a time lag between orbital conjunction and photometric maximum. Table 4 shows that the inclination i for the best fit solution increases slightly when the spectroscopic or photometric T_0-epochs are adopted (see Table 4).

The accuracy of the orientation of the line of nodes Ω suffers mainly from the uncertainty in the T_0-epoch. As the binary axis rotates on the average $360°/P$ = 0.65° per day, the difference of 42 days between polarimetric and photometric T_0 corresponds

to a difference of almost 30° in Ω. According to Table 4 we may thus adopt for Ω a value in the range Ω = 130° − 170°.

The best fit solutions for the polarimetric orbit show also systematic trends if they are computed from different wavelength sections in the Raman lines. The blue line wing provides results with higher inclination i (Table 4). It also shows much less scatter (σ in Table 4) in the measured polarization angles. Both trends are visible in the λ6825 and λ7082 components and do not depend qualitatively on the different T_0-epoch.

The proposed scattering models for the Raman lines in symbiotic systems (Schmid & Schild 1994; Harries & Howarth 1996b, 1996c; Schmid 1996) suggest that the polarization in the blue line wing is the best tracer of the binary motion. According to these models the photons in the blue wing are produced predominantly in the neutral region between the two stars. There the scattering H^0-atoms in the giant's wind are expected to move towards the O VI source. This produces, due to the Doppler effect, a blue shifted Raman photon. Contrary to this the photons in the red line wing originate predominately in the outer wind region, which recedes from the O VI source. Thus the inner region producing the line photons in the blue wing is relatively small and the corresponding scattering geometry is probably well aligned with the binary axis. The geometry of the outer region, on the other hand, is expected to be more fluffy and the resulting polarization angle is subject to considerable geometric compensation effects (see e.g. Schmid & Schild 1994 for details). This model thus provides also a plausible explanation for the larger scatter in the polarization angles of the red line wing (Table 4).

Based on the "standard" scattering model we may give more credit to the fit solution from the polarization angles of the blue part in the Raman lines.

6.1.2. Adopted results

The uncertainties discussed in the previous section prevent a determination of accurate values for the inclination i and the orientation of the orbital plane Ω. Nevertheless we can adopt values which are in agreement with the polarimetric measurements and our understanding of the Raman scattering problem. However we have to allow, due to the various uncertainties, quite large error ranges. Our preferred values are:

$i = 120°$ $\quad (105° - 140°)$

$\Omega = 150°$ $\quad (130° - 170°)$

For considerably more accurate results we have to gain more insight into the second order effects which produce irregular (or not understood) deviations of $\sigma \approx 10°$ from the orbital fits.

6.2. On stellar masses

The orbital inclination is an important parameter for the derivation of stellar masses in binary systems. In this section we examine the constraints set by the above orbital inclination on the stellar masses. The relationship between orbital quantities and masses can be described for single-lined spectroscopic binaries, like AG Dra, by the mass function m_f

$$m_\mathrm{f} = \frac{1}{2\pi G} P K^3 (1-\epsilon^2)^{3/2} = \frac{(M_\mathrm{h} \sin i)^3}{(M_\mathrm{h} + M_\mathrm{c})^2} ,$$

where G stands for the gravitational constant, P the orbital period, K the radial velocity semi-amplitude for the cool giant, ϵ the eccentricity, i the inclination and M_h, M_c the masses of the hot and cool component, respectively. Rearrangement gives the hot components mass M_h in terms of the total system mass and orbital parameters:

$$M_\mathrm{h} = \frac{K}{\sin i} (M_\mathrm{h} + M_\mathrm{c})^{2/3} \Big(\frac{P}{2\pi G}\Big)^{1/3} (1-\epsilon^2)^{1/2} .$$

The period $P = 554 \pm 3$ from the light curve (see Sect. 3) and the eccentricity $\epsilon < 0.3$ from radial velocity measurements (Mikolajewska et al. 1995; Smith et al. 1996) are sufficiently well known but the uncertainties connected with the parameters K, $\sin i$ and the total system mass $M_\mathrm{sys} = M_\mathrm{h} + M_\mathrm{c}$ lead to substantial error bars.

For the orbital parameters we adopt $K = 5.0 \pm 0.5$ km/s and $\sin i = 0.80 \pm 0.16$. The radial velocity semi-amplitude of the cool giant was determined by Mikolajewska et al. (1995) and Smith et al. (1996). The measurement of K suffers from a relatively large intrinsic jitter in radial velocities, which is typical for red giants with high luminosity (see the discussion in Smith et al. 1996). The uncertainties in our orbital inclination i have been discussed in Sect. 6.1.1. We believe that the adopted errors for i and K are rather conservative. The inclination i introduces in the M_h determination a twofold larger uncertainty than K.

For the total system mass we assume $M_\mathrm{sys} = 1.5 \pm 0.5$ $M_\odot$. A higher system mass > 2 $M_\odot$ is not plausible for AG Dra, because it is an old halo object with low metallicity and high radial velocity. A lower system mass < 1 $M_\odot$ is not compatible with the stellar masses expected for a hot component (white dwarf) and a red giant both with luminosities of the order $L \approx 1000$ $L_\odot$ (Mikolajewska et al. 1995).

With the above values the mass of the hot component becomes $M_\mathrm{h} = 0.32$ $M_\odot$ Extreme values for the hot components mass, when applying the full error ranges for K, $\sin i$ and M_sys, are $M_\mathrm{h} = 0.17$ $M_\odot$ and $M_\mathrm{h} = 0.52$ $M_\odot$. The mass for the cool component is $M_\mathrm{c} = 1.18$ $M_\odot$ (using $K = 5$ km/s, $\sin i = 0.80$, $M_\mathrm{sys} = 1.5$ $M_\odot$) and the corresponding extreme values are 0.83 $M_\odot$ and 1.48 $M_\odot$ respectively.

6.3. The white dwarf mass and the Barium star scenario

Recent studies on AG Dra give evidence based on different observational facts that the hot component is a white dwarf (e.g. Mikolajewska et al. 1995; Smith et al. 1996; Greiner et al. 1996). Therefore, we take the hot component to be a hot white dwarf without repeating the argumentation of these papers.

The estimated mass of $M_{\rm h}$ = 0.32 $M_\odot$ (0.17 $M_\odot < M_{\rm h} <$ 0.52 $M_\odot$) is relatively low for a white dwarf. Surveys of single white dwarf masses give mean values around 0.60 $M_\odot$ and only about 10% of the objects have a mass below 0.40 $M_\odot$ (e.g. Bergeron et al. 1992; Bragaglia et al. 1995). A mass below the "canonical" helium flash mass M_f = 0.45 $\pm$ 0.05 $M_\odot$ (Sweigart & Gross 1978) would suggest that the hot component in AG Dra is a helium white dwarf. This interpretation implies that the present hot component lost or transfered its envelope during its evolution on the red giant branch before reaching a sufficiently high core mass for helium burning. However, such an interpretation excludes the Barium star scenario for AG Dra as proposed by Smith et al. (1996). They determined for the red giant in AG Dra a clear overabundance of s-process elements. The standard interpretation for this abundance pattern is that mass transfer occurred from an AGB-star (earlier evolutionary state of the present white dwarf) to the companion which is now the cool giant. This scenario for Barium star type binaries requires that the present white dwarf is a CO white dwarf with a mass above the helium shell flash threshold M_f. The uncertainties of our mass estimate does not exclude a mass $M_{\rm h} \gtrsim M_f$ and therefore a CO white dwarf in AG Dra. However, this would require a radial velocity amplitude around $K \approx$ 5.5 km/s and $i \approx 135^\circ$ and a relatively high mass for the cool component $M_{\rm c} \approx 1.5$ $M_\odot$. These values would still be compatible with our measurements, but they are pushed to the "allowed" limit.

We conclude that the derived mass for the white dwarf in AG Dra is relatively low but due to the large uncertainty not in conflict with the Barium star scenario. Further studies are needed to put more stringent constraints on the WD mass in AG Dra. The Barium star scenario is very attractive for explaining the s-process element overabundances of AG Dra. However, it is conceivable that the measured s-process element overabundances could also be intrinsic to the cool giant being now on the AGB and undergoing helium shell flashes. That the cool giant in AG Dra could be an AGB star is supported by various observational parameters, like IR colours, low surface gravity, large radial velocity jitter, or large line widths which are all similar to those of bright giants in globular clusters (see Mikolajewska et al. 1995; Smith et al. 1996). A measurement (or an upper limit) of the abundance of the unstable s-process element Tc could tell, whether the s-process elements are produced now in the cool giant (Tc present) or whether the s-process elements were acquired in an earlier mass transfer episode (Tc decayed in the meantime and is therefore absent). Thus, the s-process element overabundances measured by Smith et al. (1996) does not rule out the presence of a low mass helium white dwarf in AG Dra with $M_{\rm h} \lesssim 0.4$ $M_\odot$.

7. Discussion

We present a series of spectropolarimetric observations of the Raman scattered O VI emission lines $\lambda\lambda$6825,7082 of the AG Dra symbiotic system. As expected, the polarization signal in the Raman lines shows temporal changes which, in the case of the polarization angle, are linked to the orbital motion. This confirms the basic Raman scattering model in which the O VI photons originate from the hot component's side and are Raman scattered by H^0-atoms in a region near to the cool component.

The temporal changes of the polarization angle in the Raman lines are dominated by the binary orbit. Particularly the blue portion of the profile remains, even under outburst conditions, a surprisingly good tracer of orbital motion. The red portion of the angle profile also clearly reflects this motion but with an increased scatter. The polarization angles show residuals from the formal orbital solution that are larger than the observational errors. There appears to be a second order effect which makes the scattering geometry wobble around the true binary axis by at least a few degrees. Such deviations have also been observed in the quiescent symbiotic SY Mus (Harries & Howarth 1996a) and may be a feature which is common to many symbiotic systems. Changing asymmetries or occultation effects may account for such an effect. In this respect, it is interesting to note that we observe angle rotations across the Raman line profile. Such rotations can only be produced by asymmetries in the scattering geometry. The fact that we see transitions from clockwise to anti-clockwise rotation (from blue to red) indicate that such asymmetries can be reversed.

The percentage polarization in the Raman lines appears to vary in an unpredictable way and is certainly strongly affected by both, orbital motion and the outburst properties. Percentage polarization is susceptible to e.g. fluctuations in the concentration of neutral hydrogen. At present we have little detailed knowledge about the nebular matter distribution in quiescent symbiotics and the situation is even worse for outbursting objects. The observed percentage polarization profiles potentially contain a lot of information about the neutral matter distribution however additional information e.g. about the O VI profiles is necessary before firm conclusions can be drawn.

The outburst changed the Raman scattering conditions in at least two ways. Firstly, the O VI irradiation increased strongly, associated with changes in the line profile. Secondly, the O VI Raman line intensity remained constant or even decreased in spite of the enhanced irradiation. This suggests that a significant part of the previously Raman-active neutral scattering region was removed during outburst. Further support for this interpretation comes from the sudden increase of nebular emission indicating that a large amount of the surrounding neutral material became newly ionized.

It is beyond the scope of this observational paper to construct a comprehensive model for the scattering geometry in AG Dra. In Schmid (1996) a series of model calculations for the Raman scattered O VI lines is presented and a critical comparison between model results and observations of symbiotic systems is given. The observed properties of the Raman lines in AG Dra, like the integrated line polarization and the polarization structure, suggest a scattering geometry between the Schmid-models XB3 and XC3. Such a model also explains, if the low inclination $\sin i$ of AG Dra is considered, the steady, time-dependent rotation of the polarization angle and the relatively small temporal variations in the line flux and the percentage polarization. The effects of complicating factors on the Raman line structure,

like outbursts, density fluctuations, or 3-dimensional scattering geometries have not been investigated numerically. The interpretation of such effects is therefore more speculative.

The close relationship between polarization angle and orbital motion, even in an outbursting object, enables the estimation of the orbital inclination i and the orientation of the line of nodes Ω. For AG Dra we find an inclination of $i = 120°$ and $\Omega = 150°$. The uncertainty range for i is rather large ($105° - 140°$) due to irregular deviations from a mean scattering geometry. Using published radial velocity data and with plausible assumptions on the total system mass we obtain a mass of the hot white dwarf between 0.17 $M_\odot$ and 0.52 $M_\odot$. This mass is rather low for white dwarfs which have a mean value of ≈ 0.6 $M_\odot$. Unfortunately, our measurement of the orbit inclination is not accurate enough for distinguishing between a $M_{\rm h} \lesssim 0.4$ $M_\odot$ helium white dwarf and a $M_{\rm h} \approx 0.5$ $M_\odot$ CO white dwarf. Further studies on the Raman scattering problem in symbiotic systems may clarify the nature of the observed second order effects in the polarization angle variations. This would help to determine more accurately the component in the rotation of the polarization angle which is only induced by the orbital motion. This would put more stringent limits on the white dwarf mass in the AG Draconis system.

Acknowledgements. We are indebted to the La Palma support astronomers who carried out the service observations. We are particularly grateful to René Rutten and Vik Dhillon. We thank Urs Mürset for valuable discussions and comments on the manuscript. This work was financially supported by the Swiss National Science Foundation.

References

Allen D.A., 1980, MNRAS, 190, 75
Bergeron P., Saffer R.A., Liebert J., 1992, ApJ, 394, 228
Bragaglia A., Renzini A., Bergeron P., 1995, ApJ, 443, 735
Brown J.C., McLean I.S., Emslie A.G., 1978, A&A, 68, 415
Friedjung M., Stencel R.E., Viotti R., 1983, A&A, 126, 407
Garcia M.R., Kenyon S.J., 1988, in: The Symbiotic Phenomenon, IAU Coll. 103, J. Mikolajewska et al. (eds), Kluwer, p. 27
Garnavich P.M., Trammell S.R., 1995, BAAS, 27, 1399
Granslo B.H., Poyner G., Takenaka Y., Schmeer P., 1994, IAU Circ. 6009
Greiner J., Bickert K., Luthardt R., et al., 1996, in: Supersoft X-ray sources, J. Greiner (ed.), Springer, p. 267
Harries T.J., Howarth I.D., 1996a, A&A, 310, 235
Harries T.J., Howarth I.D., 1996b, A&AS, 119, 61
Harries T.J., Howarth I.D., 1996c, A&A, in press
Hric L., Skopal A., Urban Z., et al., 1993, Contrib. Astron. Obs. Skalnate Pleso, 23, 73
Hric L., Skopal A., Chochol D., et al., 1994, Contrib. Astron. Obs. Skalnate Pleso, 24, 31
Iijima T., Vittone A., Chochol D., 1987, A&A, 178, 203
Kafatos M., Meier S.R., Martin I., 1993, ApJS, 84, 201
Kaler J.B., 1987, AJ, 94, 437
Kaler J.B., Stoehr C.A., Hartkopf W.I., et al., 1987, AJ, 94, 452
Kenyon S.J., Livio M., Mikolajewska J., Tout C.A., 1993, ApJ, 407, L81
Lutz J.H., Lutz T.E., Dull J.D., Kolb D.D., 1987, AJ, 94, 463
Meinunger L., 1979, IBVS, No. 1611
Mikolajewska J., Kenyon S.J., Mikolajewski M., Garcia M.R. Polidan R.S., 1995, AJ, 109, 1289
Mürset U., Nussbaumer H., Schmid H.M., Vogel M., 1991, A&A, 248, 458
Robert C., Moffat A.F.J., Bastien P., St-Louis N., Drissen L., 1990, ApJ 359, 211
Rudy R.J., Kemp J.C., 1978, ApJ, 221, 200
Schild H., Schmid H.M., 1992, Gemini - Newsletter RGO, 37, 4; reprinted in Current Science, 63, 536
Schild H., Schmid H.M., 1996, A&A, 310, 211
Schmid H.M., 1989, A&A, 211, L31
Schmid H.M., 1992, A&A, 254, 224
Schmid H.M., 1994, A&A, 284, 156
Schmid H.M., 1996, MNRAS, 282, 511
Schmid H.M., Nussbaumer H., 1993, A&A, 268, 159
Schmid H.M., Schild H., 1990, A&A, 236, L13
Schmid H.M., Schild H., 1994, A&A, 281, 145 (Paper I)
Schulte-Ladbeck R., 1985, A&A, 142, 333
Schulte-Ladbeck R., Aspin C., Magalhaes A.M., Schwarz H.E., 1990, A&AS, 86, 227
Skopal A., 1994, IBVS, No. 4096
Skopal A., 1996, (personal communication)
Skopal A., Hric L., Urban Z., et al., 1992, Contrib. Astron. Obs. Skalnate Pleso, 22, 131
Skopal A., Hric L., Chochol D., et al., 1995, Contrib. Astron. Obs. Skalnate Pleso, 25, 53
Smith V.V., Cunha K., Jorissen A., Boffin H. 1996, A&A, in press
Sweigart A.V., Gross P.G., 1978, ApJS, 36, 405
Viotti R., Ricciardi O., Ponz D., et al., 1983, A&A, 119, 285
Viotti R., Altamore A., Baratta G.B., Cassatella A., Friedjung M., 1984, ApJ, 283, 226

This article was processed by the author using Springer-Verlag LaTeX A&A style file *L-AA* version 3.